JACS
JOURNAL OF THE AMERICAN CHEMICAL SOCIETY

Article

pubs.acs.org/JACS

Temperature-Induced Structural Phase Transitions in a Two-Dimensional Self-Assembled Network

Matthew O. Blunt,*[,†,§] Jinne Adisoejoso,[†,∥] Kazukuni Tahara,[‡] Keisuke Katayama,[‡] Mark Van der Auweraer,*[,†] Yoshito Tobe,*[,‡] and Steven De Feyter*[,†]

[†]Department of Chemistry, Division of Molecular Imaging and Photonics, Laboratory of Photochemistry and Spectroscopy, KU Leuven - University of Leuven, Celestijnenlaan 200 F B2404, B-3001 Leuven, Belgium

[‡]Division of Frontier Materials Science, Graduate School of Engineering Science, Osaka University, Toyonaka, Osaka 560-8531, Japan

Supporting Information

ABSTRACT: Two-dimensional (2D) supramolecular self-assembly at liquid−solid interfaces is a thermodynamically complex process producing a variety of structures. The formation of multiple network morphologies from the same molecular building blocks is a common occurrence. We use scanning tunnelling microscopy (STM) to investigate a structural phase transition between a densely packed and a porous phase of an alkylated dehydrobenzo[12]annulene (DBA) derivative physisorbed at a solvent−graphite interface. The influence of temperature and concentration are studied and the results combined using a thermodynamic model to measure enthalpy and entropy changes associated with the transition. These experimental results are compared to corresponding values obtained from simulations and theoretical calculations. This comparison highlights the importance of considering the solvent when modeling porous self-assembled networks. The results also demonstrate the power of using structural phase transitions to study the thermodynamics of these systems and will have implications for the development of predictive models for 2D self-assembly.

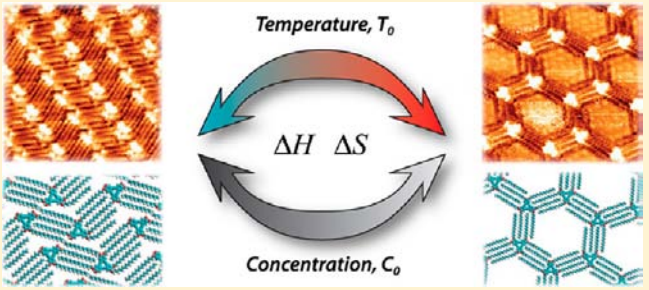

INTRODUCTION

Supramolecular self-assembly at liquid−solid interfaces produces numerous two-dimensional (2D) architectures[1−3] with potential applications in nanotechnology, guest molecule adsorption,[4−8] chiral ordering/induction,[9−11] 2D polymers,[12,13] molecular electronics,[14,15] and functional materials.[16−18] To properly implement these applications, control over network morphology is required. This control is often obtained using a qualitative knowledge of which morphology is produced for a particular system, followed by stepwise variations of molecular structure and system parameters. While effective, this process is complex and time-consuming. The ability to accurately predict the thermodynamic equilibrium structure for a particular system would be a great advantage. Such prediction is difficult because even simple systems consisting of a combination of a single network molecule and a solvent often display more than one phase of 2D packing when deposited on a surface.[19−39] Structures can be true polymorphs, the same components combining in different 2D crystal structures, or structural phases with varying levels of solvent coadsorption or different ratios of components for multicomponent systems. Which structure is observed depends on the solvent,[19−21] substrate,[22,23] concentration,[24−29] temperature,[30−37] and for multicomponent systems the ratios of the different components.[38,39]

The thermodynamic equilibrium for self-assembly represents a balance of the enthalpy gained during formation against the entropic cost of constraining the molecules. Molecular simulations are widely employed to estimate enthalpy values for 2D self-assembly.[5,7,10,14,22,23,31,33,38] Estimated values for entropy changes associated with self-assembly are less common and can be obtained using molecular modeling[40,41] or by theoretical calculations.[31,42,43] Methods used for estimating enthalpy and entropy values are often forced to simplify molecular systems, a common example being simulations that ignore the presence of substrate or solvent to reduce computation time. It is vital that the required level of detail is used in simulations to produce accurate results. The only way to check the accuracy of such simulations is to develop experimental methods to measure enthalpy and entropy values that can be directly compared to modeled results.

Systems with multiple structural phases provide an ideal testing ground for thermodynamic models of 2D self-assembly as they often display transitions between phases in response to changes in system parameters.[28,29,31,38,44] Transitions can be tracked using STM, and several examples of simple thermodynamic models have been developed to describe such systems.[24,28,29,31,38] Lei et al.[28] put forward a model for a transition between high density and low density phases in response to reducing concentration. In later work, Bellec et al.[29]

Received: June 4, 2013
Published: July 5, 2013

 © 2013 American Chemical Society dx.doi.org/10.1021/ja405585s | J. Am. Chem. Soc. 2013, 135, 12068−12075

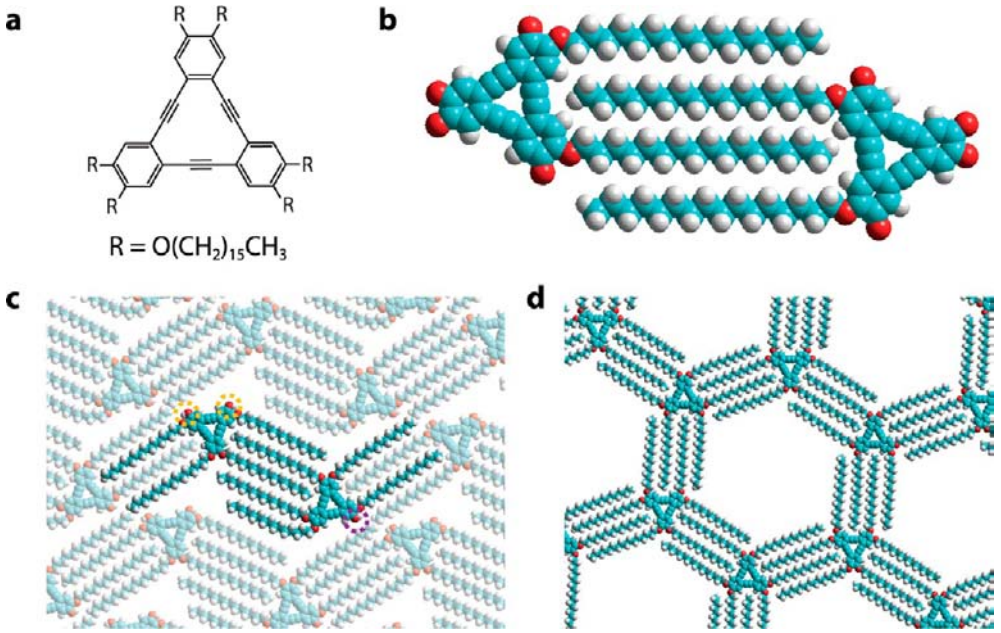

Figure 1. Chemical structure of DBA-OC16 and molecular models for the porous and linear phases. (a) Chemical structure of DBA-OC16. (b) Molecular model showing interdigitation of alkoxy chains between adjacent DBA-OC16 molecules. (c) Molecular model of the linear phase for DBA-OC16. The linear phase consists of rows of closely packed DBA-OC16 molecules. Alternate rows of DBA molecules have four and five of their six alkoxy chains adsorbed on the surface. For clarity, only the adsorbed alkoxy chains are included in the structure. For the DBA molecules with five of their six chains adsorbed on the surface, four of the chains adopt a standard interdigitation pattern, as shown in (b), while the fifth chain adopts a bent configuration so that most of its length can lie parallel to other adsorbed chains. The dashed circles mark the locations of desorbed alkoxy chains, orange for the DBA with two desorbed chains and purple for the DBA with one desorbed chain. (d) Molecular model of the porous phase for DBA-OC16. Each DBA molecule has all six of its alkoxy chains adsorbed on the surface and interdigitated with chains from adjacent DBA molecules forming a network of hexagonal nanopores.

expanded this model to include the effect of domain size and discuss the importance of kinetic effects and thermal history. Despite the number of studies of self-assembly at the liquid–solid interface, there have been relatively few that investigate the effect of temperature.[30−37,44−47] One of the most important[31] detailed a reversible transition between porous and densely packed phases where the porous phase was stabilized at low temperatures by coadsorbed solvent molecules. However, no previous study has used such a transition to measure enthalpy or entropy changes associated with 2D self-assembly.

We describe a reversible transition between two phases of a monocomponent molecular system. STM was used to collect submolecular resolution images at a liquid–solid interface and, to our knowledge, provide the first detailed investigation of the temperature–concentration phase space for a structural transition in a 2D self-assembled network. Furthermore, STM results were combined with a thermodynamic model of the transition in an unprecedented way to produce experimentally measured values for enthalpy and entropy changes associated with this type of 2D structural transition. These experimentally derived thermodynamic values were compared to similar results obtained from molecular mechanics (MM) simulations and theoretical calculations. Reasonable agreement between experiment and simulation is obtained for both enthalpy and entropy values when coadsorbed solvent molecules are included in the MM simulations. In addition to simply including coadsorbed solvent molecules solvation effects need to be incorporated into any thermodynamic model. The degree to which molecular motion is restricted following self-assembly, and hence the change in entropy, are also of key importance. These results go beyond the investigation of a single combination of molecule, substrate, and solvent by showcasing ideas and methodologies that are generally applicable to a broad range of molecular systems and are important for the future study and application of 2D molecular self-assembly. They demonstrate the power of using structural phase transitions to probe the thermodynamics of 2D self-assembly, and they highlight the importance of entropy changes that accompany the formation of ordered 2D molecular networks.

The molecular system discussed here consists of alkylated dehydrobenzo[12]annulene (DBA) physisorbed at the liquid–solid interface between 1,2,4-trichlorobenzene (TCB) and highly oriented pyrolytic graphite (HOPG). Each DBA molecule consists of a triangular aromatic core functionalized with six alkoxy chains (see Figure 1a). DBA self-assembly has previously been studied with STM at the liquid–solid interface.[28,48] DBA networks are stabilized through van der Waals interactions between interdigitated alkoxy chains on adjacent molecules (Figure 1b). DBAs can form two distinct structures:[28] a high density linear phase in which 50% of the DBA molecules have one alkoxy chain desorbed from the surface and 50% have two chains desorbed (Figure 1c); and a low density porous phase in which all six chains are adsorbed and the DBA forms an array of hexagonal nanopores (Figure 1d). Both structures are described in detail in the Supporting Information.

■ EXPERIMENTAL SECTION

All STM experiments were performed using a PicoSPM (Agilent) system operating in constant-current mode with the tip immersed in the supernatant liquid. STM tips were prepared by mechanical cutting of Pt/Ir wire (80%/20%, diameter 0.25 mm). Substrates consisted of

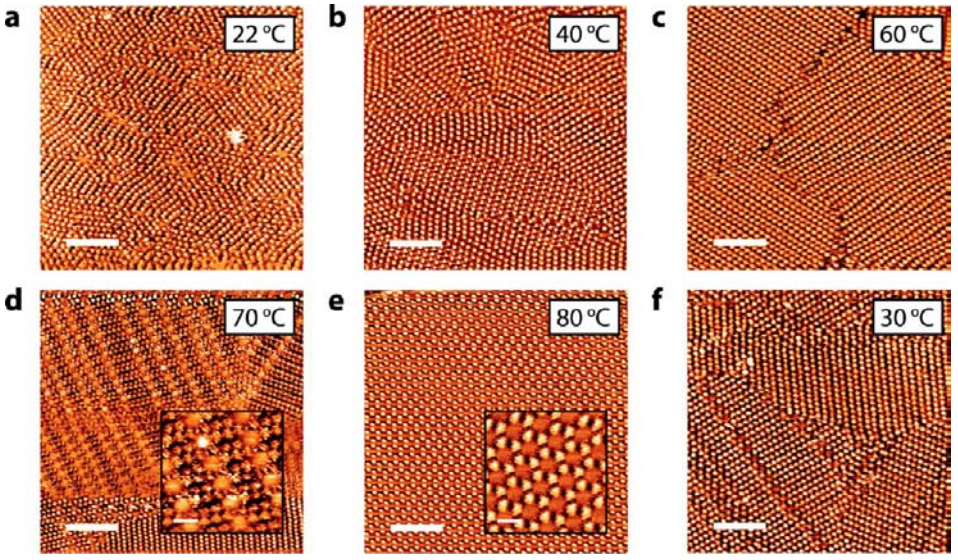

Figure 2. A set of typical STM images for a sequential heating experiment using a DBA-OC16 solution in TCB with a concentration of 5.8×10^{-4} mol/L. (a) Initial deposition of solution was carried out with the substrate and solution held at 22 °C (295 K). The temperature was then raised in 10 °C steps with STM images collected at each temperature. Images are shown for temperatures of 40 °C (313 K) (b), 60 °C (333 K) (c), 70 °C (343 K) (d), and 80 °C (353 K) (e). The system was then allowed to cool naturally to 30 °C (303 K) and imaged (f). The insets to (d) and (e) display enlarged regions of the DBA network at these temperatures. Scale bars: (a–c) 16 nm; (d–f) 20 nm; (d,e insets) 4 nm. The STM images were collected using tunneling set points between 20 and 50 pA and a tip bias of +1.2 V.

HOPG (grade ZYB, Advanced Ceramics Inc., Cleveland, OH). 1,2,4-Trichlorobenezene (TCB, Sigma-Aldrich, 99%) was used as solvent without further purification. A dehydrobenzo[12]annulenes (DBA) derivative with alkoxy chains consisting of 16 carbons (DBA-OC16) was synthesized according to previously reported methods.[28,48] A stock solution with concentration of 5.75×10^{-4} mol/L was produced by weighing out 3 mg of solid and dissolving in 3 mL of TCB. The error in weighing was assumed to be that of the weighing scales (±0.5 mg) giving a relative error of ±17%. This stock solution was then diluted to give a range of the concentrations down to 4.60×10^{-6} mol/L. Because of the accuracy of using weighing scales to determine quantities of solution and additional solvent, the dilution steps did not significantly increase the error and a relative error value of ±17% was used for all subsequent concentrations.

Immediately prior to use, HOPG substrates were freshly cleaved using adhesive tape. The HOPG substrate was then placed onto an in situ temperature control stage, which consisted of a copper base plate with an inbuilt resistive heating element and thermocouple. The temperature of the heating stage was controlled via a feedback loop using a Lakeshore model 331 temperature controller. This arrangement provides an accessible temperature range from room temperature to ~80 °C (353 K). At temperatures greater than this, the thermal instability of the system and the rate of solvent evaporation became too large to obtain good quality STM images. A liquid cell constructed of PTFE was used to hold ~50 μL of the desired solution on the HOPG substrate.

For sequential heating experiments, all depositions were carried out with the solution and substrate held at room temperature. Following deposition, different temperatures were investigated by heating/cooling the system with the DBA solution in place. After STM images had been collected at a particular temperature, the STM tip was retracted 50 μm from the surface and the temperature raised/lowered to the next desired value at a rate of 10 °C/min. Once at the target temperature, the sample was allowed to settle for 2 min before the tip was re-engaged and scanning recommenced. In some cases, both heating and cooling data were obtained; however, in the majority of experiments, only heating data from room temperature to 80 °C (353 K) were collected. For individual temperature experiments, both the bare HOPG substrate and the solution were preheated to the desired temperature prior to deposition. Following STM imaging, the solution was removed and the HOPG substrate and the liquid cell cleaned and the HOPG substrate freshly cleaved before repeating the experiment for a different temperature with fresh solution. To minimize the influence of solvent evaporation, a fixed time of 20 min was spent imaging at each temperature for the sequential heating experiments and 60 min at each temperature for the individual temperature experiments. This restriction on the time spent collecting images at each temperature meant that for some temperatures only a single image of adequate resolution was collected, while for other temperatures several images were obtained.

The fractional coverage of porous phase at each temperature was calculated by collecting as many STM images as possible within the allotted time. These images were collected at different locations across the sample surface to obtain a statistically reliable sample of the network structure. The porous phase was defined as any region of DBA network that consisted of a complete hexagonal pore. These regions were marked on the images by hand in a graphical software package, and the fractional coverage of porous phase was calculated for the resulting binary images. A value of the fractional coverage of porous phase for each temperature was then calculated by taking an average of the values from each image collected at that temperature. The error in the fractional coverage at each temperature was assigned as the standard deviation of these values unless only a single image had been obtained for a particular temperature, in which case an error value of ±0.1 was used as this was approximately the average of the combined error values.

■ RESULTS AND DISCUSSION

Figure 2a–f shows a set of typical STM images for a sequential heating experiment where a DBA-OC16 solution (5.8×10^{-4} mol/L) was deposited at 22 °C (295 K) and the temperature was increased in steps up to 80 °C (353 K) and then allowed to cool to 30 °C (303 K). At 22 °C (295 K), the network forms predominantly the linear phase with many small domains 5–20 nm in size and a high density of packing defects and domain boundaries (Figure 2a). On heating to 60 °C (333 K) (Figure 2c), domain size has increased to between 50 and 200 nm. This domain coarsening is reminiscent of 2D Ostwald ripening where systems evolve to minimize energetically unfavorable domain boundaries. Similar results were described by Bellec et

dx.doi.org/10.1021/ja405585s | J. Am. Chem. Soc. 2013, 135, 12068–12075

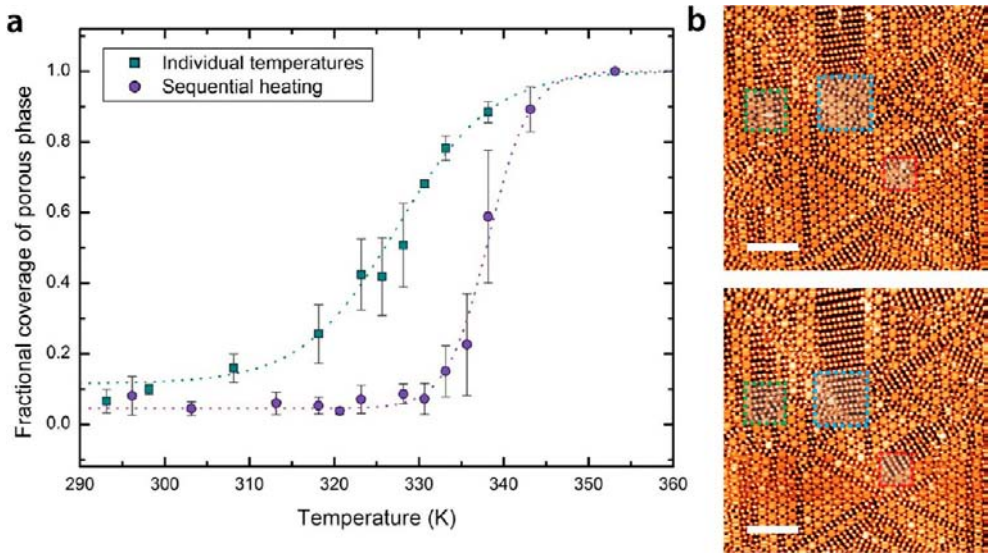

Figure 3. The influence of thermal history on the linear-to-porous transition. (a) Fractional coverage of porous phase as a function of temperature for DBA-OC16 in TCB (1.15×10^{-4} mol/L) for the individual temperature and sequential heating experiments. Sigmoidal fits are included for both data sets. (b) Consecutive STM images (top image acquired first) of the same surface area. The images were acquired at 50 °C (323 K) in the individual temperature experiment. The time elapsed between completion of the two images was ~2.5 min. The color coded boxes mark regions where the DBA network has rearranged between images. STM scale bars are 20 nm, and the images were collected using a tunneling set point of 40 pA and a tip bias of +0.65 V.

al.[29] for a similar molecule and have been reported for various 2D supramolecular networks.[49,50]

At ~70 °C (343 K) (Figure 2d), a structural rearrangement begins as lines of porous phase, one hexagonal pore in width, grow within domains of the linear phase. The inset to Figure 2d shows a high-resolution image of one of these structures. Following an increase in temperature to 80 °C (353 K), the network undergoes a complete transition to the porous phase (Figure 2e). The resulting porous structure is highly ordered with domain boundaries only observed at HOPG steps. The system was allowed to cool naturally to 30 °C (303 K) where it underwent a transition back to the linear phase (Figure 2f). By repeating cycles of heating and cooling, it was possible to cross this transition multiple times.

Bellec et al.[29] highlighted the role played by kinetic effects in 2D molecular self-assembly and the importance of controlling a system's thermal history. To investigate kinetic effects in the DBA networks, individual temperature experiments were carried out. DBA-OC16 solutions (1.15×10^{-4} mol/L) were preheated to a desired temperature and deposited on a substrate held at the same temperature. The samples were then imaged to ascertain the fractional coverage of porous phase. This was repeated for temperatures from room temperature to 65 °C (338 K). The variation of fractional coverage of porous phase with temperature for the individual temperature experiments and the sequential heating experiment displayed in Figure 2 are both presented in Figure 3a.

Despite the fact that the two experimental data sets underwent different periods of time spent at different temperatures (see methods section and Supporting Information for details), we are able to make a qualitative comparison between them. At low temperatures in the sequential heating experiments, the surface is almost completely covered by the linear phase. With increasing temperature, this situation continues unchanged until a sharp transition to the porous phase is observed at the transition temperature. In comparison, for the individual temperature experiments, the fraction of the surface covered by porous phase increases gradually with increasing temperature from room temperature upward.

Closer inspection of STM images from the individual temperatures experiments shows that at temperatures below the transition temperature in the sequential heating experiments, ~64 °C (~337 K), porous domains continue to evolve during scanning. Figure 3b shows consecutive STM images of the same surface area for the individual temperatures experiment at 50 °C (~323 K). The network structure locally rearranges between images; several examples of this rearrangement are marked in Figure 3. A similar set of consecutive STM images obtained at 55 °C (328 K) is given in the Supporting Information. Each observed rearrangement of the network proceeds in the same direction, porous to linear. This gradual rearrangement of the porous phase in the individual temperature experiments suggests that it is a kinetically trapped structure. When deposition is carried out at elevated temperatures, but still below the transition temperature as seen in the sequential heating experiments, the growth of the porous phase is favored despite it not being the equilibrium structure. Once the network is fully formed, the porous phase becomes kinetically trapped and slowly restructures into the linear phase. These results mirror those of Bellec et al.[29] who showed that increased temperature during deposition favored the formation of a porous phase and led to the formation of kinetically trapped structures. These results give us confidence that the linear phase observed below the transition temperature in the sequential heating experiments is an equilibrium structure. In turn, this suggests that the porous phase formed by raising the temperature above the transition temperature is also an equilibrium structure. Given that we have a transition between two equilibrium structures, we can use thermodynamics to model this process.

To investigate the influence of concentration, sequential heating experiments were performed for DBA-OC16 concentrations between 2.30×10^{-5} and 2.87×10^{-4} mol/L. Some of the results for these experiments are shown in Figure 4a along

dx.doi.org/10.1021/ja405585s | J. Am. Chem. Soc. 2013, 135, 12068−12075

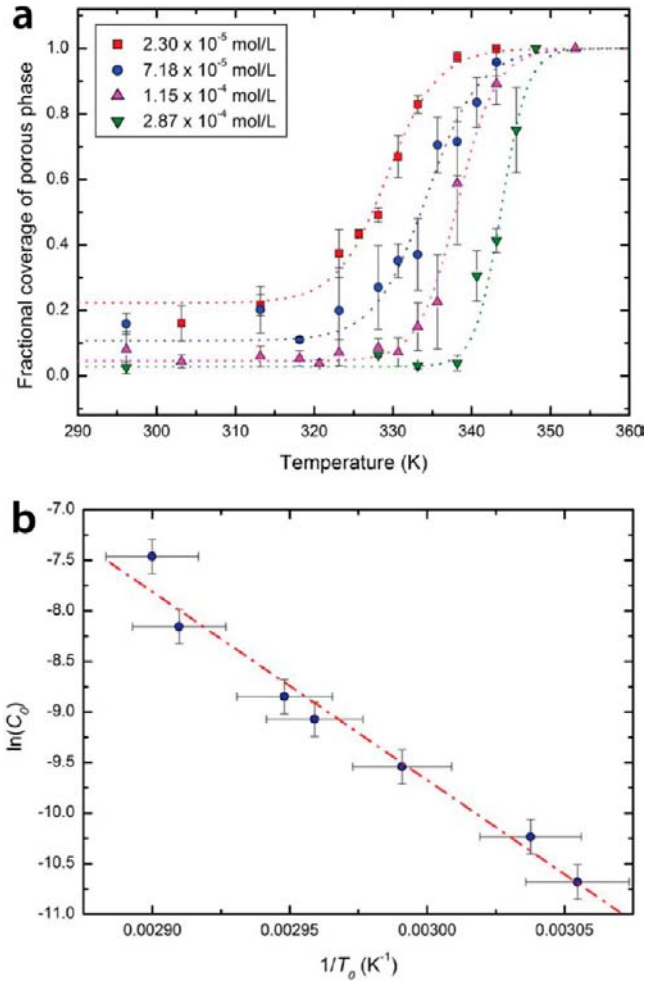

Figure 4. Fractional coverage of the porous phase as a function of temperature for different concentrations. (a) Plots of the fractional coverage of porous phase as a function of temperature for DBA-OC16 in TCB at concentrations between 2.30×10^{-5} and 2.87×10^{-4} mol/L. The dashed lines represent sigmoidal fits to the data. The transition temperature (T_0) is measured by taking the temperature at which the sigmoidal fit equals a fractional coverage of 0.5. (b) Plot of $\ln(C_0)$ against $1/T_0$ for DBA concentrations between 2.30×10^{-5} and 5.75×10^{-4} mol/L. Error bars were calculated using a relative error of 17% for the concentration values and ±2 °C for the temperature values. The dashed red line represents a linear fit to the data.

with sigmoidal fits to the data. Complete experimental data can be found in the Supporting Information. Sigmoid curves were fitted with their upper bound constrained at 1 and the lower bound free, mimicking a transition between a partial coverage of linear phase and a complete coverage of porous phase.

Lowering the concentration makes the transition more gradual and shifts it to lower temperatures. A previously developed model for linear-to-porous transitions in a DBA network was based on a system under thermodynamic control where molecules in the two phases are in equilibrium with molecules in solution.[28] This model treated molecules as noninteracting and predicted a gradual transition between the linear and porous phases with decreasing concentration. An expansion of this model[29] included interactions between molecules by taking into account the domain size. This improved model predicted a sharp transition due to the entropic cost of forming ordered domains as opposed to noninteracting molecules in random orientations. For domain sizes equivalent to those seen experimentally, the transition becomes step-like, occurring at a single critical concentration (C_0). The coexistence of linear and porous phases away from C_0 was attributed to kinetic trapping. By careful control over the thermal history, this sharp transition was demonstrated experimentally.[29]

At C_0 the change in free energy going from a unit area of linear to a unit area of porous phase is equal to zero. This can be used to derive an expression for C_0, eq 1. This equation is conceptually similar to the thermodynamic model described by Bellec et al.[29] with the addition of an explicit term to model the entropy loss associated with the coadsorption of solvent molecules. A detailed derivation of eq 1 is given in the Supporting Information.

$$\ln C_0 = \frac{1}{k_B T_0}\left(-\Delta H^0_{lin} + \frac{(\Delta H^0_{por} - \Delta H^0_{lin})}{(m-1)}\right) + \frac{\Delta S^0_{lin}}{k_B} - \frac{(\Delta S^0_{por} - \Delta S^0_{lin})}{(m-1)k_B} - \frac{19\Delta S^0_{TCB}}{2(m-1)k_B} \quad (1)$$

where ΔH^0_{lin} and ΔH^0_{por} are the enthalpy changes per DBA molecule for desorption from the surface in, respectively, the linear and porous phases. These enthalpy values include all of the different interactions within the network: molecule–substrate, molecule–molecule, and molecule–solvent. ΔS^0_{lin} and ΔS^0_{por} are the entropy changes per DBA associated with desorption from the linear and porous phases, respectively, and ΔS^0_{TCB} is the entropy change per TCB for desorption from the surface. The factor of 19/2 in eq 1 arises because there are 19 TCB molecules and 6 DBA molecules per pore in the porous phase. Each DBA is shared between three adjacent pores, so the number of TCB per DBA is 19/2. The parameter m is the ratio of surface molecular densities of DBA in the porous and linear phases. Equation 1 is based on the fact that at C_0 the enthalpy cost of converting a unit area of linear phase into a unit area of porous phase is exactly offset in the free energy by the gain in entropy. From eq 1, we see that C_0 is temperature dependent. If increasing the temperature also increases C_0, we have a simple explanation for the transition. If the DBA concentration is above C_0, the network adopts the linear phase, assuming it has been allowed to reach equilibrium. As the temperature is raised, the DBA concentration remains constant, but C_0 increases. If C_0 surpasses the actual concentration, the system undergoes a linear to porous transition.

From eq 1, a plot of $\ln(C_0)$ against $1/T_0$ (T_0 being the transition temperature) should produce a straight line. We obtain values for T_0 and C_0 from the DBA-OC16 sequential temperature experiments at various concentrations (Figure 4a). T_0 is measured as the temperature at which the sigmoid fits equal a fractional coverage of 0.5. Seven sets of T_0 and C_0 values were obtained for concentrations between 2.30×10^{-5} and 5.75×10^{-4} mol/L. Figure 4b shows a plot of $\ln(C_0)$ against $1/T_0$. The gradient and intercept of a linear fit to these data were obtained and multiplied by the Boltzmann constant ($k_B = 1.381 \times 10^{-23}$ m^2 kg s^{-2} K^{-1}) to give eqs 2 and 3:

$$-\Delta H^0_{lin} + \frac{(\Delta H^0_{por} - \Delta H^0_{lin})}{(m-1)} = (-2.57 \pm 0.16) \times 10^{-19}\ \text{J} \quad (2)$$

dx.doi.org/10.1021/ja405585s | J. Am. Chem. Soc. 2013, 135, 12068–12075

$$\frac{\Delta S^0_{lin}}{k_B} - \frac{(\Delta S^0_{por} - \Delta S^0_{lin})}{(m-1)k_B} - \frac{19\Delta S^0_{TCB}}{2(m-1)k_B} = (6.38 \pm 0.48) \times 10^{-22}\ \mathrm{J\ K^{-1}} \quad (3)$$

To test the validity of these experimental results, MM simulations were performed to calculate ΔH^0_{lin} and ΔH^0_{por} (see the Supporting Information for details). Previous studies have shown the importance of coadsorbed solvent molecules when developing thermodynamic models for porous molecular networks.[31,38,51] High-resolution STM images of the porous phase of DBA-OC16 (Figure 5a) show that each pore contains 19 coadsorbed TCB molecules in a hexagonal close packed arrangement. One of the pores in Figure 5a contains a single bright and poorly resolved feature. A tentative explanation for this is that an excess DBA molecule from solution was partially immobilized within the pore. Similar single bright features within pores were observed in other images but were extremely rare occurring in less than 0.1% of all observed pores.

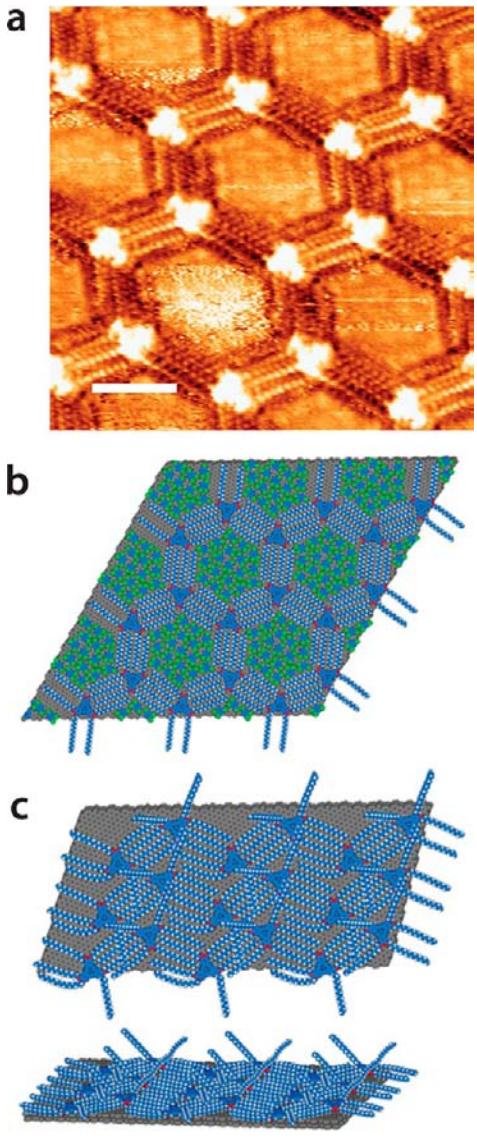

Figure 5. Solvent coadsorption in the porous phase and molecular mechanics (MM) simulations of the porous and linear phases. (a) High-resolution STM image showing 19 TCB molecules coadsorbed in a hexagonally close packed arrangement with each pore of the porous DBA-OC16 network. Scale bar 2.4 nm, set point of 20 pA, and tip bias +0.65 V. (b) MM optimized structure for the porous phase of DBA-OC16 on HOPG with 19 coadsorbed TCB molecules per unit cell. (c) MM optimized structure (top and side views) for the linear phase of DBA-OC16 on HOPG. The MM simulations of the linear phase include all of the alkoxy chains, adsorbed and desorbed.

Combined STM images of the linear and porous phases with the underlying HOPG were used to build accurate starting configurations for MM simulations that included coadsorbed solvent molecules for the porous phase and desorbed alkoxy chains for the linear phase (see the Supporting Information). Optimized structures for the phases are displayed in Figure 5b,c. Analysis of MM simulations gave values for ΔH^0_{lin} and ΔH^0_{por} that were combined with a value for m = 2.42 obtained in a previous study of DBA-OC16[28] to give a value for the gradient term of -1.78×10^{-18} J. This simulated value falls outside the error bounds of the experimentally measured value ($(-2.57 \pm 0.16) \times 10^{-19}$ J). This difference may result because the MM simulations do not include the bulk solvent layer. Enthalpy values obtained from MM simulations represent the difference in enthalpy between molecules in vacuum and molecules in the adsorbed network. However, in reality the enthalpy values are the difference between molecules in solution and molecules in the adsorbed network. Accounting for solute−solvent and solvent−solvent interactions is a key factor in reliably modeling enthalpy changes in real experimental systems.

The restriction of molecular motion that accompanies self-assembly results in the loss of translational, rotational, conformational, and vibrational entropy. Translational and rotational entropy was estimated using a method suggested by Whitesides and co-workers.[42] The conformational entropy was estimated using a bond counting method also developed by Whitesides et al.[43] For a more detailed description of these calculations, see the Supporting Information. The estimated entropy changes were ΔS^0_{lin} = 928.9 J mol^{-1} K^{-1}; ΔS^0_{por} = 1094.9 J mol^{-1} K^{-1}; and ΔS^0_{TCB} = 232.8 J mol^{-1} K^{-1}. These values were combined to produce a theoretical estimate for the entropy term in eq 3 of $(-1.24 \pm 0.16) \times 10^{-21}$ J K^{-1}. This estimated value lies well outside of the error bounds of the experimental value ($(6.38 \pm 0.48) \times 10^{-22}$ J K^{-1}) and has the opposite sign.

The major contribution to the theoretical estimate is the entropy lost by coadsorbing TCB molecules in the porous phase, outweighing the entropy gained by desorption of DBA from the linear phase. The experimental and theoretical enthalpy values both suggest that the enthalpy change for the linear to porous transition is positive. A transition with a positive change in enthalpy can only be favored if the corresponding change in entropy is also positive. This suggests the experimental value for the entropy change is more accurate and relevant than the theoretical estimate.

One explanation for the discrepancy between theory and experiment is that some molecules do not lose all of their entropy on adsorption. The estimated values assume a complete restriction of molecular motion for any molecule or segment of a molecule that is adsorbed on the surface. This seems reasonable for DBA-OC16 molecules; they appear as well-defined features in the STM images with individual methyl groups clearly resolved (Figure 5a). However, in exactly the same STM images, TCB molecules appear as diffuse features. This lack of spatial resolution suggests the TCB molecules remain mobile within the pores and retain some of their

dx.doi.org/10.1021/ja405585s | J. Am. Chem. Soc. 2013, 135, 12068−12075

translational and rotational entropy. In addition, the theoretical values of the rotational entropy for both DBA and TCB molecules in solution will be overestimated by the methodology used here (see the Supporting Information). These effects lead to the value of ΔS^0_{TCB} being overestimated by the theoretical calculations.

Reducing ΔS^0_{TCB} would move the theoretical estimate of eq 3 closer to the experimental value. Entropic effects have recently been demonstrated in 2D supramolecular self-assembly; the entropic cost of alkyl chain adsorption can lead to destabilization of different network morphologies;[52] the free rotation of molecules can stabilize 2D molecular networks through increased rotational entropy.[53] A note of caution should be made concerning the calculation of conformational entropy.[43] It has been shown that even small variations in the torsional barriers experienced by individual bonds can cause this method to produce erroneous results leading to an overestimation of the loss in conformational entropy.[54,55] More accurate methods for determining the conformational entropy based on molecular dynamics simulations are available.[32,40,41,51] However, despite being computationally extremely intensive, these methods provide little insight into the relationship between molecular structure and entropy change upon adsorption.

CONCLUSIONS

We have performed a detailed investigation of the influence of temperature and concentration on the transition between two structural phases of self-assembled networks of DBA molecules at the liquid−solid interface. The results of these studies were combined with a thermodynamic model of the transition in a novel method to measure values for the enthalpy and entropy change associated with the transition. These results represent the first detailed STM investigation of how temperature and concentration influence 2D self-assembly at a liquid−solid interface and the first direct measurement of thermodynamic values associated with such a self-assembly process. Comparison between these experimental results and simulation/theory demonstrated the importance of the solvent when building thermodynamic models of self-assembly. MM simulations and theoretical calculations limited to molecules in the monolayer directly adsorbed on the surface lead to a reasonable approximation of enthalpy and entropy values. In order to produce more accurate modeled values for enthalpy and entropy changes the solvation of molecules and the degree to which molecular motion is restricted during self-assembly both need to be quantified.

Structural transitions are both useful as a method for producing highly ordered 2D supramolecular networks and interesting from a theoretical standpoint as they provide a window into the complex thermodynamic landscape of self-assembly at liquid−solid interfaces. To develop accurate modeling techniques for 2D molecular self-assembly at liquid−solid interfaces, we need to experimentally test simulated enthalpy and entropy values for numerous different molecular systems. Detailed STM investigation of the temperature and concentration dependence of structural transitions, as demonstrated by this work, is a broadly applicable technique for 2D molecular self-assembly that allows exactly this type of measurement to be obtained. Such experiments provide a way to test the viability of different theoretical and simulation methods and open the way for the development of more accurate modeling techniques. In turn, these modeling methods will have a profound impact on the application of 2D supramolecular self-assembly in nanotechnology.

ASSOCIATED CONTENT

Supporting Information

High-resolution STM images of porous and linear phases; images analysis methods; complete data sets for all concentration experiments; details of molecular mechanics simulations; details of derivation of the thermodynamic model; and theoretical estimates of entropy values. This material is available free of charge via the Internet at http://pubs.acs.org.

AUTHOR INFORMATION

Corresponding Author

m.blunt@ucl.ac.uk; mark.vanderauweraer@chem.kuleuven.be; tobe@chem.es.osaka-u.ac.jp; steven.defeyter@chem.kuleuven.be

Present Addresses

[§]Department of Chemistry, University College London, WC1H 0AJ, United Kingdom.

[∥]Department of Physics, The Hong Kong University of Science and Technology, Clear Water Bay, Hong Kong, China.

Notes

The authors declare no competing financial interest.

ACKNOWLEDGMENTS

M.O.B. would like to acknowledge the Marie Curie Actions program for the award of an Intra-European Fellowship (piefga-2009-254009, FUNSURF). We also want to thank the Interuniversity Attraction Poles Programme (P7/05) initiated by the Belgian Science Policy Office and the Research Fund of KU Leuven through GOA 11/003, and the Fund of Scientific Research - Flanders (FWO). J.A. is grateful to the Agency for Innovation by Science and Technology in Flanders (IWT). This work is supported by a Grant-in-Aid for Scientific Research from the Ministry of Education, Culture, Sports, Science, and Technology, Japan (21245012, 23111710).

REFERENCES

(1) De Feyter, S.; De Schryver, F. C. *J. Phys. Chem. B* **2005**, *109*, 4290−4302.

(2) Bonifazi, D.; Mohnani, S.; Llanes-Pallas, A. *Chem.-Eur. J.* **2009**, *15*, 7004−7025.

(3) Slater (Nee Phillips), A. G.; Beton, P. H.; Champness, N. R. *Chem. Sci.* **2011**, *2*, 1440−1448.

(4) Griessl, S. J. H.; Lackinger, M.; Jamitzky, F.; Markert, T.; Hietschold, M.; Heckl, W. M. *Langmuir* **2004**, *20*, 9403−9407.

(5) Wu, D. X.; Deng, K.; Zeng, Q. D.; Wang, C. *J. Phys. Chem. B* **2005**, *109*, 22296−22300.

(6) Lei, S.; Surin, M.; Tahara, K.; Adisoejoso, J.; Lazzaroni, R.; Tobe, Y.; De Feyter, S. *Nano Lett.* **2008**, *8*, 2541−2546.

(7) Blunt, M.; Lin, X.; Gimenez-Lopez, M. D. C.; Schröder, M.; Champness, N. R.; Beton, P. H. *Chem. Commun.* **2008**, 2304−2306.

(8) MacLeod, J. M.; Ivasenko, O.; Fu, C.; Taerum, T.; Rosei, F.; Perepichka, D. *J. Am. Chem. Soc.* **2009**, *131*, 16844−16850.

(9) Chen, T.; Yang, W.-H.; Wang, D.; Wan, L.-J. *Nat. Commun.* **2013**, *4*, 1389.

(10) Tahara, K.; Yamaga, H.; Ghijsens, E.; Inukai, K.; Adisoejoso, J.; Blunt, M. O.; De Feyter, S.; Tobe, Y. *Nat. Chem.* **2011**, *3*, 714−719.

(11) Elemans, J. A. A. W.; De Cat, I.; Xu, H.; De Feyter, S. *Chem. Soc. Rev.* **2009**, *38*, 722−736.

(12) Dienstmaier, J. F.; Gigler, A. M.; Goetz, A. J.; Knoche, P.; Bein, T.; Lyapin, A.; Reichlmaier, S.; Heckl, W. M.; Lackinger, M. *ACS Nano* **2011**, *5*, 9737−9745.

(13) Russell, J. C.; Blunt, M. O.; Garfitt, J. M.; Scurr, D. J.; Alexander, M.; Champness, N. R.; Beton, P. H. *J. Am. Chem. Soc.* **2011**, *133*, 4220−4223.
(14) Okawa, Y.; Mandal, S. K.; Hu, C.; Tateyama, Y.; Goedecker, S.; Tsukamoto, S.; Hasegawa, T.; Gimzewski, J. K.; Aono, M. *J. Am. Chem. Soc.* **2011**, *133*, 8227−8233.
(15) Wang, Y.; Kröger, J.; Berndt, R.; Hofer, W. A. *J. Am. Chem. Soc.* **2009**, *131*, 3639−3643.
(16) Xue, Y.; Zimmt, M. B. *J. Am. Chem. Soc.* **2012**, *134*, 4513−4516.
(17) Ciesielski, A.; Palma, C. A.; Bonini, M.; Samori, P. *Adv. Mater.* **2010**, *22*, 3506−3520.
(18) Pace, G.; Ferri, V.; Grave, C.; Elbing, M.; von Hänisch, C.; Zharnikov, M.; Mayor, M.; Rampi, M. A.; Samorì, P. *Proc. Natl. Acad. Sci. U.S.A.* **2007**, *104*, 9937−9942.
(19) Kampschulte, L.; Lackinger, M.; Maier, A. K.; Kishore, R. S.; Griessl, S.; Schmittel, M.; Heckl, W. M. *J. Phys. Chem. B* **2006**, *110*, 10829−10836.
(20) Miao, X. R.; Xu, L.; Li, Z. M.; Deng, W. L. *J. Phys. Chem. C* **2011**, *115*, 3358−3367.
(21) Chen, T.; Wang, D.; Zhang, X.; Zhou, Q.; Zhang, R.; Wan, L. *J. Phys. Chem. C* **2010**, *114*, 533−538.
(22) Balandina, T.; Tahara, K.; Sändig, N.; Blunt, M. O.; Adisoejoso, J.; Lei, S.; Zerbetto, F.; Tobe, Y.; De Feyter, S. *ACS Nano* **2012**, *6*, 8381−8389.
(23) Piot, L.; Marchenko, A.; Wu, J.; Müllen, K.; Fichou, D. *J. Am. Chem. Soc.* **2005**, *127*, 16245−16250.
(24) Ahn, S.; Matzger, A. J. *J. Am. Chem. Soc.* **2010**, *132*, 11364−11371.
(25) Dienstmaier, J. F.; Mahata, K.; Walch, H.; Heckl, W. M.; Schmittel, M.; Lackinger, M. *Langmuir* **2010**, *26*, 10708−10716.
(26) Tahara, K.; Okuhata, S.; Adisoejoso, J.; Lei, S.; Fujita, T.; De Feyter, S.; Tobe, Y. *J. Am. Chem. Soc.* **2009**, *131*, 17583−17590.
(27) Nguyen, T. N. H.; Gopakumar, T. G.; Hietschold, M. *J. Phys. Chem. C* **2011**, *115*, 21743−21749.
(28) Lei, S.; Tahara, K.; De Schryver, F. C.; Van der Auweraer, M.; Tobe, Y.; De Feyter, S. *Angew. Chem.* **2008**, *120*, 3006−3010.
(29) Bellec, A.; Arrigoni, C.; Schull, G.; Douillard, L.; Fiorini-Debuisschert, C.; Mathevet, F.; Kreher, D.; Attias, A. J.; Charra, F. *J. Chem. Phys.* **2011**, *134*, 124702.
(30) Marie, C.; Silly, F.; Tortech, L.; Müllen, K.; Fichou, D. *ACS Nano* **2010**, *4*, 1288−1292.
(31) Gutzler, R.; Sirtl, T.; Dienstmaier, J. F.; Mahata, K.; Heckl, W. M.; Schmittel, M.; Lackinger, M. *J. Am. Chem. Soc.* **2010**, *132*, 5084−5090.
(32) Saiz-Poseu, J.; Faraudo, J.; Figueras, A.; Alibes, R.; Busqué, F.; Ruiz-Molina, D. *Chem.-Eur. J.* **2012**, *18*, 3056−3063.
(33) Li, Y.; Liu, C.; Xie, Y.; Li, X.; Li, X.; Fan, X.; Deng, K.; Zeng, Q.; Wang, C. *Phys. Chem. Chem. Phys.* **2013**, *15*, 125−128.
(34) Li, C. J.; Zeng, Q. D.; Liu, Y. H.; Wan, L. J.; Wang, C.; Wang, C. R.; Bai, C. L. *ChemPhysChem* **2003**, *4*, 857−859.
(35) Shen, Y. T.; Zhu, N.; Zhang, X. M.; Deng, K.; Feng, W.; Yan, Q.; Lei, S.; Zhao, D.; Zeng, Q. D.; Wang, C. *Chem.-Eur. J.* **2011**, *17*, 7061−7068.
(36) Adisoejoso, J.; Tahara, K.; Lei, S.; Szabelski, P.; Rżysko, W.; Inukai, K.; Blunt, M. O.; Tobe, Y.; De Feyter, S. *ACS Nano* **2012**, *6*, 897−903.
(37) Jahanbekam, A.; Vorpahl, S.; Mazur, U.; Hipps, K. W. *J. Phys. Chem. C* **2013**, *117*, 2914−2919.
(38) Kampschulte, L.; Werblowsky, T. L.; Kishore, R. S.; Schmittel, M.; Heckl, W. M.; Lackinger, M. *J. Am. Chem. Soc.* **2008**, *130*, 8502−8507.
(39) Palma, C. A.; Bjork, J.; Bonini, M.; Dyer, M. S.; Llanes-Pallas, A.; Bonifazi, D.; Persson, M.; Samorì, P. *J. Am. Chem. Soc.* **2009**, *131*, 13062−13071.
(40) Killian, B. J.; Kravitz, J. Y.; Gilson, M. K. *J. Chem. Phys.* **2007**, *127*, 024107.
(41) Hensen, U.; Lange, O. F.; Grubmüller, H. *PLoS One* **2010**, *5*, e9179.
(42) Mammen, M.; Shakhnovich, E. I.; Deutch, J. M.; Whitesides, G. M. *J. Org. Chem.* **1998**, *63*, 3821−3830.
(43) Mammen, M.; Shakhnovich, E. I.; Deutch, J. M.; Whitesides, G. M. *J. Org. Chem.* **1998**, *63*, 3168−3175.
(44) Merz, L.; Parschau, M.; Zoppi, L.; Baldridge, K. K.; Siegel, J. S.; Ernst, K. H. *Angew. Chem., Int. Ed.* **2009**, *48*, 1966−1969.
(45) Friesen, B. A.; Bhattarai, A.; Mazur, U.; Hipps, K. W. *J. Am. Chem. Soc.* **2012**, *134*, 14897−14904.
(46) Stannard, A.; Russell, J. C.; Blunt, M. O.; Salesiotis, C.; Giménez-López, M. D. C.; Taleb, N.; Schröder, M.; Champness, N. R.; Garrahan, J. P.; Beton, P. H. *Nat. Chem.* **2012**, *4*, 112−117.
(47) English, W. A.; Hipps, K. W. *J. Phys. Chem. C* **2008**, *112*, 2026−2031.
(48) Tahara, K.; Furukawa, S.; Uji-I, H.; Uchino, T.; Ichikawa, T.; Zhang, J.; Mamdouh, W.; Sonoda, M.; De Schryver, F. C.; De Feyter, S.; Tobe, Y. *J. Am. Chem. Soc.* **2006**, *128*, 16613−16625.
(49) Stabel, A.; Heinz, R.; De Schryver, F. C.; Rabe, J. P. *J. Phys. Chem.* **1995**, *99*, 505−507.
(50) Lackinger, M.; Griessl, S.; Kampschulte, L.; Jamitzky, F.; Heckl, W. M. *Small* **2005**, *1*, 532−539.
(51) Saiz-Poseu, J.; Martínez-Otero, A.; Roussel, T.; Hui, J. K.; Montero, M. L.; Urcuyo, R.; MacLachlan, M. J.; Faraudo, J.; Ruiz-Molina, D. *Phys. Chem. Chem. Phys.* **2012**, *14*, 11937−11943.
(52) Miyake, Y.; Nagata, T.; Tanaka, H.; Yamazaki, M.; Ohta, M.; Kokawa, R.; Ogawa, T. *ACS Nano* **2012**, *6*, 3876−3887.
(53) Waldmann, T.; Klein, J.; Hoster, H. E.; Behm, R. J. *ChemPhysChem* **2013**, *14*, 162−169.
(54) Ercolani, G. *J. Org. Chem.* **1999**, *64*, 3350−3353.
(55) Chang, C. E. A.; Chen, W.; Gilson, M. K. *Proc. Natl. Acad. Sci. U.S.A.* **2007**, *104*, 1534−1539.

NOTE ADDED AFTER ASAP PUBLICATION

The notation for the entropy change terms was corrected in the text following eq 1 and the text following the discussion of Figure 5; the correct version reposted on August 14, 2013.